High strain rate deformation and resultant damage mechanisms in ultrafine-grained aluminum matrix composites

R. Vogta, Z. Zhanga, E. Huskinsb, B. Ahnc, S. Nuttc, K.T. Rameshb, E.J. Laverniaa, J.M. Schoenunga

a Department of Chemical Engineering and Materials Science, University of California, One Shields Avenue, Davis, CA 95616, USA
b Department of Mechanical Engineering, Johns Hopkins University, Baltimore, MD 21218, USA
c Department of Chemical Engineering and Materials Science, University of Southern California, Los Angeles, CA 90089, USA

Abstract:

Ultrafine-grained aluminium composites produced via cryomilling exhibited ultrahigh strength associated with considerable strain-to-failure (>14 pct.) at high strain rates (>103 s−1), but only limited strain-to-failure (~0.75 pct.) at quasi-static strain rates (10−3 s−1). The mechanisms leading to these differences in behaviour were investigated by systematic microstructural analysis of deformed and pre-deformed samples. Micro-flaw developments, including kinking, extensive axial splitting, and grain growth, were observed after high strain rate deformation, and the significance of these mechanisms is considered.

Key words: Aluminium alloys; Composites; Electron microscopy; Powder metallurgy; Dynamic compression; Axial splitting

Please cite this article as: R. Vogt, Z. Zhang, E. Huskins, B. Ahn, S. Nutt, K.T. Ramesh, E.J. Lavernia, J.M. Schoenung "**High strain rate deformation and resultant damage mechanisms in ultrafine-grained aluminum matrix composites**" Mater Sci & Engrg A 527 (2010) 5990-5996. DOI<http://dx.doi.org/10.1016/j.msea.2010.05.092>

1. Introduction

Nanostructured and ultrafine-grained (UFG) metals and alloys exhibit significant increases in strength compared to their conventional coarse-grained counterparts [1], [2], [3] and [4]. An undesirable consequence of the reduced grain size, however, is a decrease in the strain-to-failure [5] and [6]. Metal matrix composites with a nanostructured or UFG matrix have also been developed. These materials exhibit even higher strength and enhanced stiffness, but with further reduction in strain-to-failure, especially during quasi-static deformation [7] and [8]. To increase the ductility of nanostructured and UFG materials, additions of coarse-grained (CG) constituent have been used to accommodate plastic deformation [2], [5] and [9]. In previous studies, UFG aluminum matrix composites were consolidated from a blend of cryomilled and unmilled aluminum alloy (5083) powders to which boron carbide (B_4C) particulates were added. After consolidation using conventional powder metallurgy techniques, the material exhibits a complex microstructure consisting of CG and UFG matrix (with some nanocrystalline matrix phase) and micron-sized B_4C particles [5], [8] and [10]. The compressive strength of this material is on the order of 1000 MPa, which is unusually high in comparison to conventional aluminum matrix composites. The strain-to-failure for this material in quasi-static compression (10^{-3} s^{-1}) is 2.5 pct. after annealing, whereas the strain-to-failure in high strain rate (i.e., dynamic) compression (10^3–10^4 s^{-1}) is nearly 30 pct. [11]. The reported mechanisms identified to account for this observed increase in strain-to-failure were rapid nucleation and multiplication of cracks followed by shear localization [11] and [12].

Please cite this article as: R. Vogt, Z. Zhang, E. Huskins, B. Ahn, S. Nutt, K.T. Ramesh, E.J. Lavernia, J.M. Schoenung "**High strain rate deformation and resultant damage mechanisms in ultrafine-grained aluminum matrix composites**" Mater Sci & Engrg A 527 (2010) 5990-5996. DOI<http://dx.doi.org/10.1016/j.msea.2010.05.092>

In related work on brittle solids, increased inelastic deformation has been attributed to various strain localization and multiplication mechanisms. Such mechanisms include shear banding in bulk metallic glass [1] and [13], microcracking in Al_2O_3 particulate reinforced Al 6061 composites under dynamic loading [14], void nucleation and coalescence in metallic alloys [15], and axial splitting in polycrystalline tungsten [16], [17], [18], [19] and [20]. For example, Hadianfard et al. [21] reported that for an Al–Mg material tested in dynamic strain rate regimes, macroscopic shear localization appeared to be the consequence of void nucleation and growth around second phase particles (5 μm in diameter) as opposed to shear dominated damage processes in the quasi-static regime. Axial splitting was also reported to accommodate the fracture energy at high strain rates by nucleating microcracks at defect sites or second phase particles, which then developed into wing-cracks that prevented the formation of major cracks and consequential catastrophic failure [16], [20], [22] and [23].

Despite the advances yielded by the works referenced above, the deformation mechanisms in UFG composites, which often exhibit brittle fracture, are not yet fully understood. Possible reasons for this include the complexity of the microstructures and the inherent difficulties associated with sample preparation of composite materials that feature constituents that differ widely in hardness [5]. Such difficulties can and often do obscure flaws and deformation features such as axial splitting. In the present study, these challenges are addressed by employing ion beam polishing. In this polishing technique a broad ion beam is used to create a smooth and artifact-free cross section, introducing minimal strain to the specimen. The resulting sections permit clear observation of defects such as pores and cracks that are often altered and smeared by conventional abrasive polishing. Ion polished

Please cite this article as: R. Vogt, Z. Zhang, E. Huskins, B. Ahn, S. Nutt, K.T. Ramesh, E.J. Lavernia, J.M. Schoenung "**High strain rate deformation and resultant damage mechanisms in ultrafine-grained aluminum matrix composites**" Mater Sci & Engrg A 527 (2010) 5990-5996. DOI<http://dx.doi.org/10.1016/j.msea.2010.05.092>

sections are used in conjunction with SEM and TEM to systematically compare and contrast deformation microstructures produced by quasi-static and dynamic loading. Analysis of the microstructures elucidates the mechanisms by which the strain-to-failure is increased in the UFG aluminum composite at high strain rates.

2. Experimental Procedures

Gas atomized Al 5083 (Al–4.5 Mg–0.57 Mn–0.25 Fe in wt. pct.) powder (Valimet, Inc., Stockton, CA), −325 mesh particle size (<45 μm), was blended with B_4C powder (Tetrabor©, ESK Ceramics, Saline, MI), 1–7 μm particulate size, in a V-blender for 16 h. The blended powder was then cryomilled for 24 h. Details of the experimental procedures used for cryomilling have been described previously [2], [7] and [8]. Additional unmilled Al 5083 powder was then added and the mixture was V-blended again. The composite powders were canned and hot vacuum degassed at 405 °C with a 1.5 °C/min ramp rate and an 8-h hold. The vacuum level at the end of degassing was 10^{-6} Torr. The canned and degassed powders were cold isostatically pressed at 310 MPa for 5 min, then extruded at high strain rate (10^2 s^{-1}) at 525 °C.

Quasi-static mechanical testing was conducted using cubic specimens (5 mm in size) at a strain rate of 10^{-3} s^{-1}. Dynamic compression testing was conducted using a Kolsky bar at strain rates of 1750 and 2250 s^{-1} with a sample size of 3 mm × 1.75 mm high. Details of the Kolsky bar test are described elsewhere [17]. The loading direction in both the quasi-static and dynamic tests was parallel to the extrusion direction. The compression sample surfaces were polished to a 1-μm diamond finish prior to testing so that the microstructural features could be revealed directly after deformation without

Please cite this article as: R. Vogt, Z. Zhang, E. Huskins, B. Ahn, S. Nutt, K.T. Ramesh, E.J. Lavernia, J.M. Schoenung "**High strain rate deformation and resultant damage mechanisms in ultrafine-grained aluminum matrix composites**" Mater Sci & Engrg A 527 (2010) 5990-5996. DOI<http://dx.doi.org/10.1016/j.msea.2010.05.092>

additional sample polishing. These surfaces after deformation were examined using a scanning electron microscope (SEM, Philips FEI XL30 SFEG). Cross section examination was also carried out on the deformed composites by using Ga^+ ion beam images from a FIB-SEM multi-beam system (JEOL JIB-4500) on samples that were polished using an ion beam cross sectional polisher (JEOL SM-09010). Transmission electron microscopy (TEM) was carried out (Philips CM-12) on both the as-processed and dynamically deformed samples. TEM specimens were mechanically thinned to 100 μm and dimpled to 20 μm in thickness. The final perforation was performed using ion milling (Gatan PIPS-691). Average grain size, grain size distribution and average grain aspect ratio in the UFG and CG regions of each sample were determined from the TEM images on the basis of 400 matrix grains. Microhardness (Vickers) of the UFG and CG regions, respectively, was determined as the average of five indentations in each region using a 25-g load on a microhardness tester (Buehler Micromet 2004). Additional microhardness indentations were made with a 100-g load to evaluate the bonding strength of the CG-UFG interface.

3. Results

Fig. 1 shows the compressive stress-strain behavior of the B_4C-reinforced UFG aluminum composite under both quasi-static (10^{-3} s^{-1}) and dynamic (10^{+3} s^{-1}) loading rates. At quasi-static strain rates, the composite yielded at 1100 MPa and fractured at a strain of 0.75 pct. (after yielding). At dynamic strain rates, the composite yielded at ~965 MPa, followed by strain softening. However, the samples tested at dynamic strain rates did not fracture within the range of deformation possible with the test configuration. For the sample tested at 1750 s^{-1}, the deformation process was monitored using a

Please cite this article as: K. Vogt, Z. Zhang, E. Huskins, B. Ann, S. Nutt, K.T. Ramesh, E.J. Lavernia, J.M. Schoenung "**High strain rate deformation and resultant damage mechanisms in ultrafine-grained aluminum matrix composites**" Mater Sci & Engrg A 527 (2010) 5990-5996. DOI<http://dx.doi.org/10.1016/j.msea.2010.05.092>

high-speed video camera indicating the formation of shear bands, as shown in the optical images in Fig. 1b. Note that the undulations observed in the dynamic stress-strain curves after yielding are an artifact of the dynamic test.

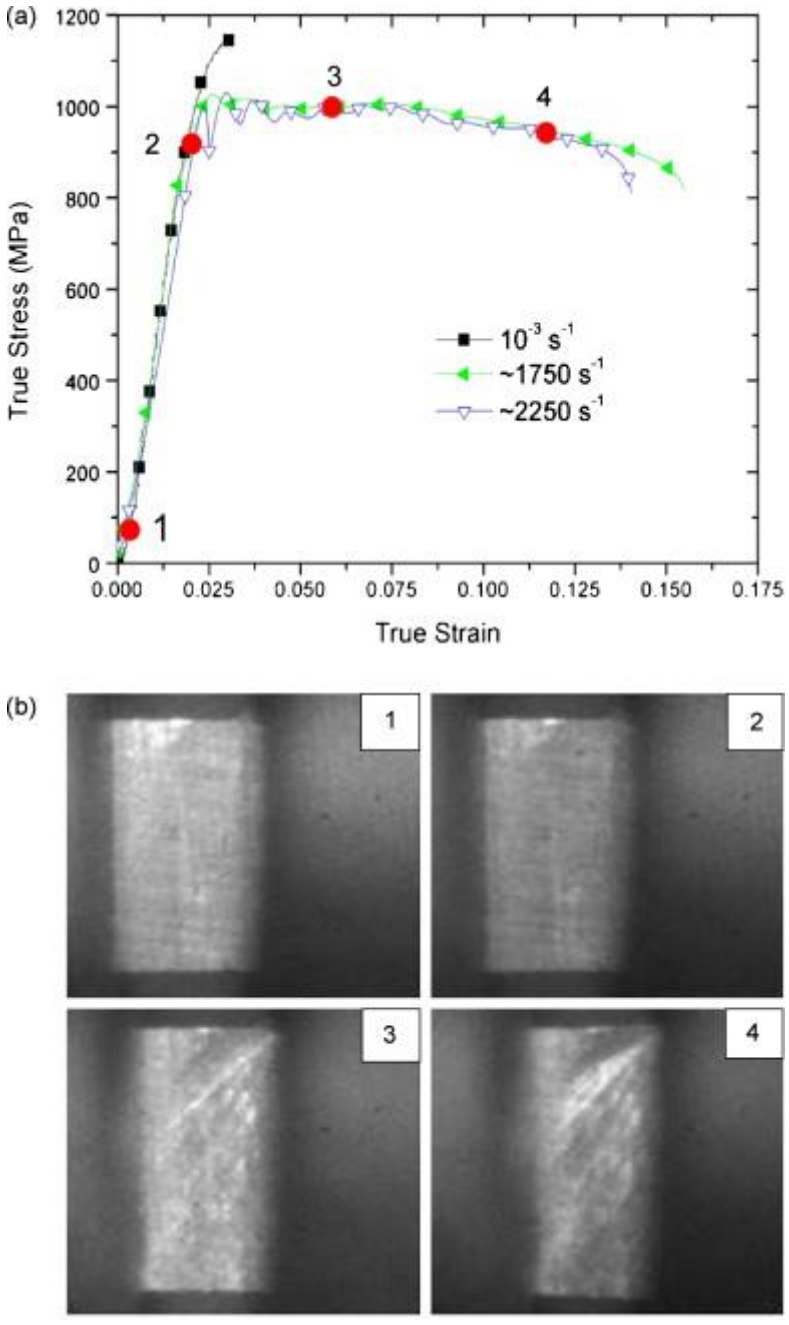

Please cite this article as: R. Vogt, Z. Zhang, E. Huskins, B. Ahn, S. Nutt, K.T. Ramesh, E.J. Lavernia, J.M. Schoenung "**High strain rate deformation and resultant damage mechanisms in ultrafine-grained aluminum matrix composites**" Mater Sci & Engrg A 527 (2010) 5990-5996. DOI<http://dx.doi.org/10.1016/j.msea.2010.05.092>

Fig. 1. (a) Quasi-static (10^{-3} s^{-1}) and dynamic compression behavior for the B_4C-reinforced ultrafine-grained aluminum composite. (b) Optical images corresponding to points 1–4, as indicated on the 1750 s^{-1} stress–strain curve taken during deformation. The samples deformed at 1750 and 2250 s^{-1} both showed evidence of apparent shear banding as seen in the progression of images 3 and 4 of the 1750 s^{-1} sample

Fig. 2 shows SEM images of samples tested at quasi-static and dynamic strain rates, viewed normal to the loading direction. The sample shown in Fig. 2a fractured along a major crack at an angle of approximately 38.5° with respect to the loading direction, and the fracture surface shows micro-roughness but no dimpling or facets (Fig. 2c). The sample in Fig. 2b, which did not fail within the strain limits of the dynamic test, exhibits microcracking that spans a few UFG/CG elongated bands, and kinking among the UFG/CG bands. Table 1 lists the Vickers hardness results for the UFG and CG regions in the as-processed material, indicating a nearly threefold increase in hardness within the UFG region when compared to that of the CG region. SEM images of a typical 100 g load indentation in the as-processed material, shown in Fig. 3, reveal delamination along the CG–UFG interface during the localized deformation.

Please cite this article as: R. Vogt, Z. Zhang, E. Huskins, B. Ahn, S. Nutt, K.T. Ramesh, E.J. Lavernia, J.M. Schoenung "**High strain rate deformation and resultant damage mechanisms in ultrafine-grained aluminum matrix composites**" Mater Sci & Engrg A 527 (2010) 5990-5996. DOI<http://dx.doi.org/10.1016/j.msea.2010.05.092>

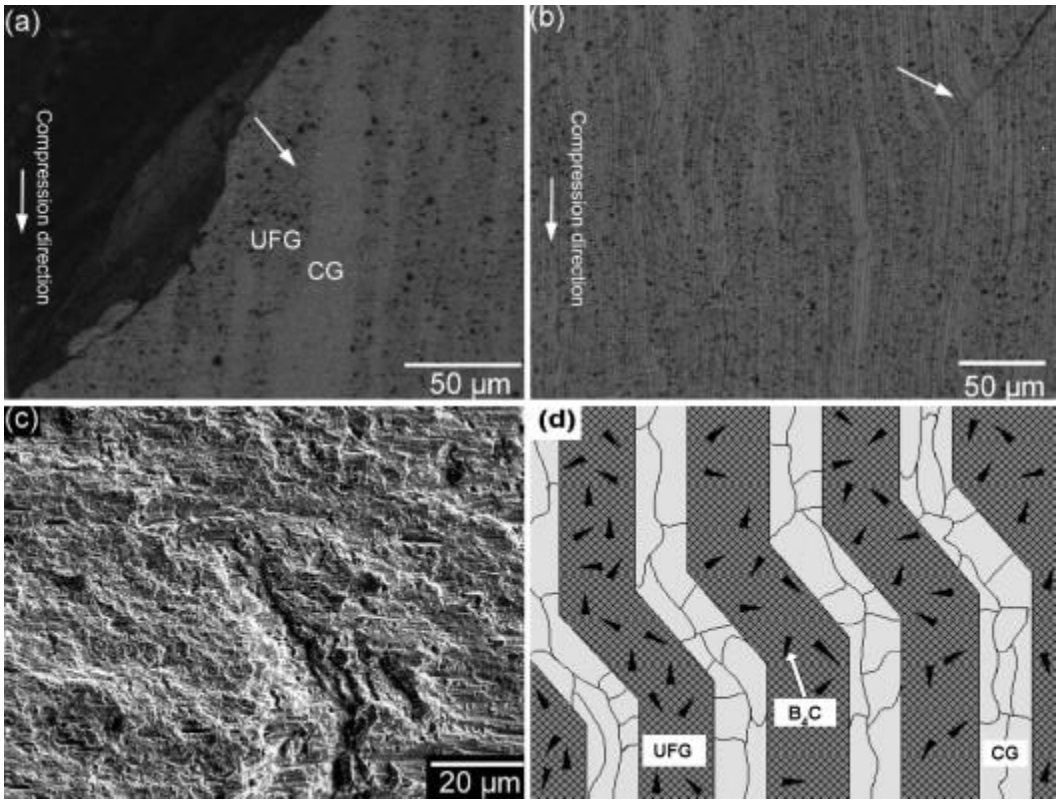

Fig. 2. SEM images of sections perpendicular to the loading direction of fractured samples deformed at (a) quasi-static, (b) dynamic (2250 s^{-1}) strain rates. Samples were polished prior to testing to ensure a flat, smooth surface for imaging. The white arrows indicate the location of cracks; the black arrows indicate the loading direction. The image in (c) illustrates the quasi-static fracture surface viewed normal to the fracture plane. The schematic in (d) illustrates the role of the microconstituents in the kinking behavior observed near the crack.

Table 1. Average microhardness values for the UFG and CG regions.

Microhardness (Vickers)		
As-processed	UFG	CG
	288 ± 20	96 ± 12

Please cite this article as: R. Vogt, Z. Zhang, E. Huskins, B. Ahn, S. Nutt, K.T. Ramesh, E.J. Lavernia, J.M. Schoenung "**High strain rate deformation and resultant damage mechanisms in ultrafine-grained aluminum matrix composites**" Mater Sci & Engrg A 527 (2010) 5990-5996. DOI<http://dx.doi.org/10.1016/j.msea.2010.05.092>

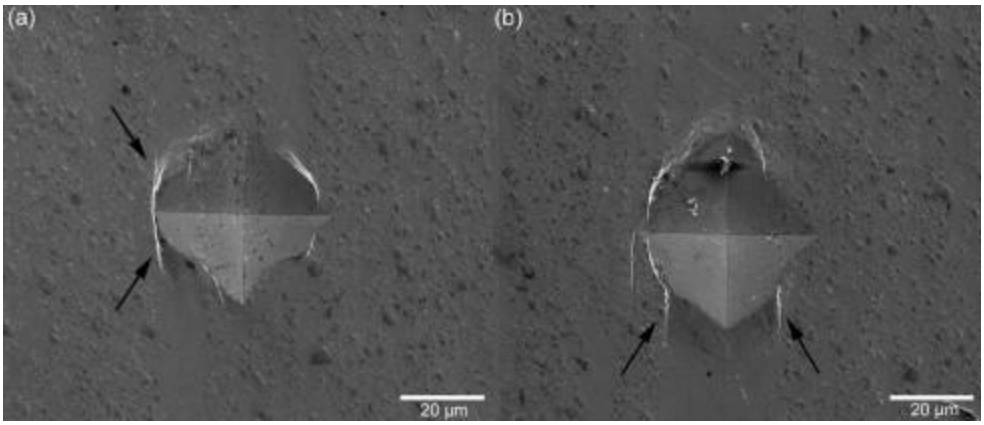

Fig. 3. Micrographs of microhardness indentations in the as-processed material: (a) indentation centered in the UFG region and, (b) indentation centered in the CG region, which highlight the presence of cracks and delamination at the UFG–CG interfaces.

Fig. 4 shows cross-sections of samples following quasi-static and dynamic testing. Multiple cracks, which align in the loading direction, appear above and below the B_4C particles. These cracks are hereafter referred to as 'axial microcracks'. The schematic inFig. 4c highlights the development of the axial microcracks in relation to the B_4C particles within the UFG region. The areal density of axial microcracks was measured from the cross section images for each test condition, as listed in Table 2.

Please cite this article as: R. Vogt, Z. Zhang, E. Huskins, B. Ahn, S. Nutt, K.T. Ramesh, E.J. Lavernia, J.M. Schoenung "**High strain rate deformation and resultant damage mechanisms in ultrafine-grained aluminum matrix composites**" Mater Sci & Engrg A 527 (2010) 5990-5996. DOI<http://dx.doi.org/10.1016/j.msea.2010.05.092>

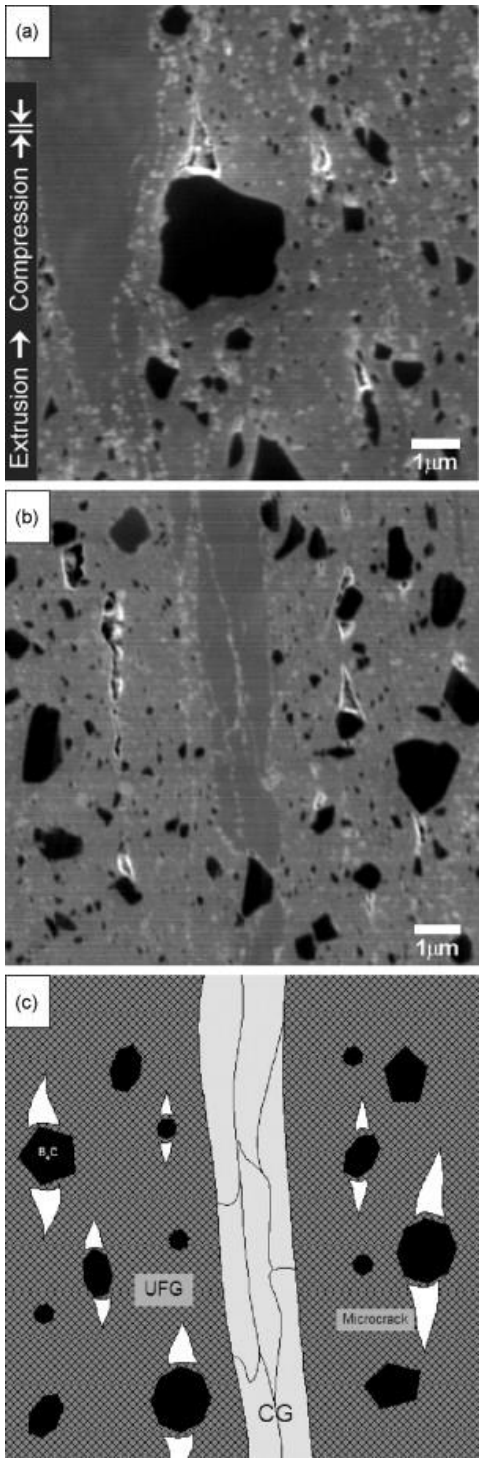

Fig. 4. SEM micrographs imaged with a Ga+ ion beam after cross sectional ion polishing showing: (a) presence of axial microcracks after quasi-static compression testing, and (b) an increase in axial

Please cite this article as: R. Vogt, Z. Zhang, E. Huskins, B. Ahn, S. Nutt, K.T. Ramesh, E.J. Lavernia, J.M. Schoenung "**High strain rate deformation and resultant damage mechanisms in ultrafine-grained aluminum matrix composites**" Mater Sci & Engrg A 527 (2010) 5990-5996. DOI<http://dx.doi.org/10.1016/j.msea.2010.05.092>

microcrack density after dynamic compression testing (2250 s^{-1}). (c) Schematic representation highlighting the location of axial microcracks near the B_4C particles in the direction of loading.

Table 2. Average axial microcrack density per unit area after compressive deformation at different strain rates.

	Axial microcrack density (m^{-2})
Quasi-static	3.4×10^{9}
Dynamic	1.6×10^{11}

TEM images of the microstructure in the as-processed condition and after dynamic testing are provided in Fig. 5 and Fig. 6, respectively, along with grain size distribution histograms and calculated values for average grain size and average aspect ratio. The narrow white region in Fig. 6b corresponds to an axial microcrack, as described above. The average grain sizes in the UFG region of the as-processed and dynamically tested samples were determined to be 156 and 211 nm, respectively; their respective aspect ratios were 1.8 and 1.6. The average grain size in the CG region in the as-processed condition was determined to be 930 nm with an aspect ratio of 2.2.

Please cite this article as: R. Vogt, Z. Zhang, E. Huskins, B. Ahn, S. Nutt, K.T. Ramesh, E.J. Lavernia, J.M. Schoenung "**High strain rate deformation and resultant damage mechanisms in ultrafine-grained aluminum matrix composites**" Mater Sci & Engrg A 527 (2010) 5990-5996. DOI<http://dx.doi.org/10.1016/j.msea.2010.05.092>

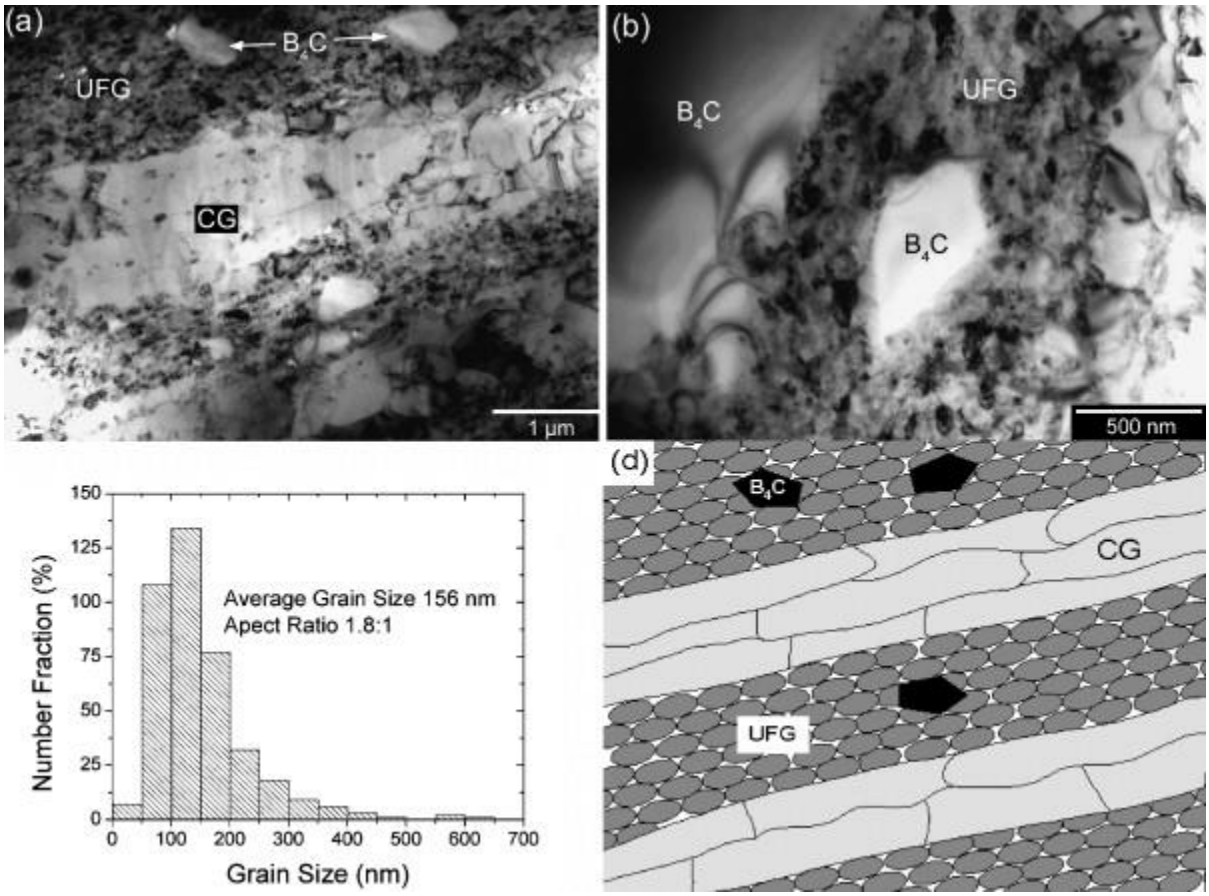

Fig. 5. TEM micrographs showing: (a) as-processed microstructure highlighting the CG band between the UFG regions that contain B_4C particles, (b) higher magnification image of as-processed microstructure highlighting the B_4C particles within the UFG region; (c) grain size distribution histogram in the UFG region as determined by measuring 400 matrix grains, and (d) schematic representation of the as-processed microstructure highlighting the texturing of the UFG/CG bands, and the elongation of the grains in the UFG region, despite the presence of the B_4C particles.

Please cite this article as: R. Vogt, Z. Zhang, E. Huskins, B. Ahn, S. Nutt, K.T. Ramesh, E.J. Lavernia, J.M. Schoenung "**High strain rate deformation and resultant damage mechanisms in ultrafine-grained aluminum matrix composites**" Mater Sci & Engrg A 527 (2010) 5990-5996. DOI<http://dx.doi.org/10.1016/j.msea.2010.05.092>

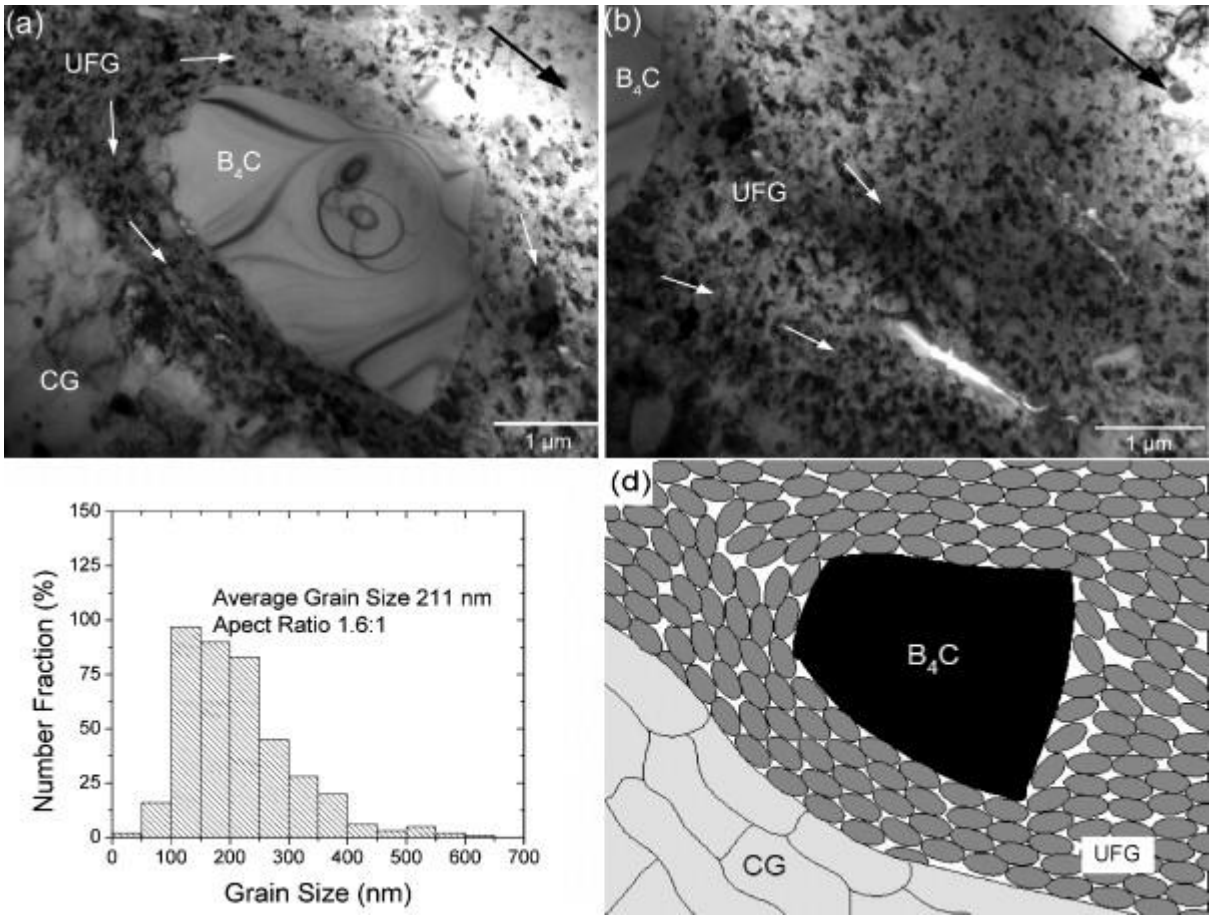

Fig. 6. TEM micrographs showing: (a) alignment of the UFG regions (arrows) around a B_4C particle after dynamic compression (2250 s^{-1}), and (b) a wing crack near a B_4C particle after dynamic compression (2250 s^{-1}); direction of compression is indicated by the dark arrow in the upper right. (c) Grain size distribution in the UFG region of the dynamically compressed sample as determined by measuring 400 matrix grains, and (d) schematic representation of the dynamically deformed UFG grain region highlighting the alignment of grains in the UFG region around a B_4C particle.

4. Discussion

The B_4C-reinforced UFG aluminum composites in the current work exhibit significant differences in mechanical response when tested under dynamic and quasi-static loading rates, as shown in Fig. 1. After quasi-static testing, the microstructure, shown in Fig. 2a, is essentially unchanged from that

Please cite this article as: R. Vogt, Z. Zhang, E. Huskins, B. Ahn, S. Nutt, K.T. Ramesh, E.J. Lavernia, J.M. Schoenung "**High strain rate deformation and resultant damage mechanisms in ultrafine-grained aluminum matrix composites**" Mater Sci & Engrg A 527 (2010) 5990-5996. DOI<http://dx.doi.org/10.1016/j.msea.2010.05.092>

of the as-processed material (Fig. 5a). Specifically, the CG regions remain distinct from the UFG regions, as illustrated in Fig. 5d. The texturing that results from the extrusion process remains clear in the quasi-static tested microstructure (Fig. 2a) and is evident from the high aspect ratio (~1.8) for the matrix grains in the B_4C-reinforced UFG region (Fig. 3c). Although axial microcracks were present after quasi-static testing (Fig. 4a), the areal density of such cracks was 1/50th that observed after dynamic testing (Table 2). It should be noted that the CG constituent was introduced to arrest crack propagation at the UFG/CG interface, as shown in Fig. 2(a). However, under quasi-static testing conditions, cracks were observed to nucleate and grow (Fig. 2a), leading ultimately to failure at a fairly low strain.

For the dynamically tested materials, however, the microstructural features are quite different from those in both the as-processed condition and after quasi-static testing. As shown in Fig. 2b, although some microcracking is detected after dynamic testing, a distinct microstructure is observed: the dynamic deformation has resulted in micro-buckling and kinking in the UFG and CG bands that lie parallel to the compression axis; such deformation behavior is not observed in the samples tested in the quasi-static regime. Kinking is often observed in unidirectional fiber-reinforced composites when loaded in axial compression [24], [25], [26], [27] and [28]. Kinking occurs when the unidirectional fibers in the composite begin to bend under an applied load. This behavior is affected by fiber misalignment, the characteristics of the interface between the fiber and the matrix, the relative stiffness values of the matrix and reinforcement, and/or their relative strength values [29]. Given the threefold difference in hardness values between the UFG and CG regions (see Table 1), the textured B_4C-reinforced UFG regions, with a dimensional width of approximately 5–10 μm and

Please cite this article as: R. Vogt, Z. Zhang, E. Huskins, B. Ahn, S. Nutt, K.T. Ramesh, E.J. Lavernia, J.M. Schoenung "**High strain rate deformation and resultant damage mechanisms in ultrafine-grained aluminum matrix composites**" Mater Sci & Engrg A 527 (2010) 5990-5996. DOI<http://dx.doi.org/10.1016/j.msea.2010.05.092>

an aspect ratio of 4:1, exhibit deformation behavior analogous to high-strength reinforcing fibers within a softer matrix. The role of the microconstituents in the kinking behavior is further illustrated in the schematic in Fig. 2d. Although kinking and micro-buckling in unidirectional ceramic-fiber-reinforced metal matrix composites have been observed during dynamic deformation in the longitudinal direction [25], [26], [27] and [28], these phenomena have not been reported for an ultrafine-grained particulate-reinforced metal matrix composite material.

Further evidence to support this analogy can be obtained by studying the interfaces between the grains in the UFG region and (a) the embedded B_4C particles and (b) the CG regions, because the interfaces strongly influence the kinking behavior in unidirectional fiber-reinforced composites [27]. Ying et al. studied the bonding between the B_4C particles and the grains in the UFG region [10] and showed a strong, clean interface that is not subject to flaws or delamination. Although microscopic characterization of the UFG–CG interface was also presented in this previous study, the strength of the interface was not considered. Therefore, to further evaluate this interface, indentations were made with a Vickers hardness tester at the UFG–CG interface region. The results, shown in Fig. 3, indicate that the interface between the UFG and CG regions is subject to delamination in the presence of a nearby stress concentration, supporting the assertion that the CG band and B_4C-reinforced UFG band can be considered to act as a soft matrix and hard reinforcement fiber, respectively. Furthermore, the B_4C-reinforced UFG region is not simply a ceramic-like brittle phase, and can thus accommodate intrinsic plastic strain deformation beyond this type of extrinsic flaw development, as described below.

Please cite this article as: R. Vogt, Z. Zhang, E. Huskins, B. Ahn, S. Nutt, K.T. Ramesh, E.J. Lavernia, J.M. Schoenung "**High strain rate deformation and resultant damage mechanisms in ultrafine-grained aluminum matrix composites**" Mater Sci & Engrg A 527 (2010) 5990-5996. DOI<http://dx.doi.org/10.1016/j.msea.2010.05.092>

The behavior within the B_4C-reinforced UFG region is considered here in more detail. Closer examination of the as-tested samples reveals axial splitting, aligned with the loading direction, after deformation (see Fig. 4). The development of axial splitting in brittle solids involves the development of axial microcracks from pre-existing flaws [20] and [22]. Under loading, the hard B_4C particles cause stress concentrations at edges and corners. When the stress field interacts with pre-existing flaws such as pores, a microcrack can form. Due to the presence of the harder B_4C phase and softer CG phase, a complex three-dimensional stress field develops within the UFG region, leading to crack splitting along the axial direction. Because of the textured microstructure (i.e., with an aspect ratio of 1.8 in the UFG region), the transverse direction, which experiences tensile stress near the particles, represents the weakest direction and a source of crack initiation. Although the axial microcracks that result from axial splitting are observed after both quasi-static and dynamic compression testing, the density of cracks is almost 50 times greater in the latter case than in the former (see Table 2). It is suggested that this increase in axial microcrack density derives from new nucleation sites near the B_4C particles, in addition to the initial flaws developing into larger axial microcracks. The finer and more extensive crack distribution observed in the dynamically loaded samples is attributed to the high loading rate and the extremely short deformation time, which leads to rapid nucleation of cracks, but little crack growth [23]. The short time scale hinders crack growth or coalescence and results in a more homogeneous distribution of cracks [18], thereby allowing the material to sustain a high strain-to-failure. In contrast, quasi-static loading results in a much smaller population of axial microcracks, which ultimately develops into a few major cracks, followed by failure at relatively low strains. Similar crack distributions and strain rate dependence has been

Please cite this article as: R. Vogt, Z. Zhang, E. Huskins, B. Ahn, S. Nutt, K.T. Ramesh, E.J. Lavernia, J.M. Schoenung "**High strain rate deformation and resultant damage mechanisms in ultrafine-grained aluminum matrix composites**" Mater Sci & Engrg A 527 (2010) 5990-5996. DOI<http://dx.doi.org/10.1016/j.msea.2010.05.092>

reported for polycrystalline tungsten, where at higher strain rates, increased strain-to-failure is attributed to axial splitting [19], and for bulk metallic glasses, where deformation at higher strain rates is accompanied by shear banding and axial splitting [18] and [22]. Axial splitting has also been observed in unidirectional fiber-reinforced composites [25].

The effective strain contribution from the axial microcracks in the dynamically tested sample can be approximated by [19] and [30]:

$$\varepsilon_{\text{microcracks}} = \frac{\sigma}{E} N \bar{c}^2 \left\{ p_1 \ln\left(\frac{l}{0.27c} + 1\right) + p_2 \sqrt{\left(\frac{l + 0.083c}{l + 0.27c}\right)} \right\} \quad (1)$$

where N is the number of axial microcracks per unit area (1.6×10^{11} m^{-2}), l is the average length of the axial microcrack (1.5 μm), c is the flaw size (0.5 μm), $\bar{c}$ is the initial flaw size (0.25 μm), and p_1 and p_2 are functions dependent on the friction coefficient and are approximated to be 0.25 and 0.38 from the literature, respectively [30]. The values for N, c, $\bar{c}$, and l were measured from SEM micrographs of cross-sectionally polished samples in the as-processed and dynamically deformed conditions. The yield stress, σ, was determined from the dynamic stress-strain curve, and Young's modulus, E, was taken to be 80.5 GPa [5]. The strain contribution from the axial microcracks was thus calculated to be 0.012 pct. (compared with a total strain > 14 pct.). Lennon and Ramesh [19] estimated a similar strain contribution value of 0.02 pct. in polycrystalline tungsten. Although the axial microcracks account for only a small portion of the effective strain contribution, the abundance of these very short cracks in the dynamically tested material in the present study precludes their coalescence. This response allows the inelastic deformation of the composite to be

Please cite this article as: R. Vogt, E. Ewing, E. Hashins, D. Kim, S. Nutt, K.T. Ramesh, E.J. Lavernia, J.M. Schoenung "**High strain rate deformation and resultant damage mechanisms in ultrafine-grained aluminum matrix composites**" Mater Sci & Engrg A 527 (2010) 5990-5996. DOI<http://dx.doi.org/10.1016/j.msea.2010.05.092>

carried more homogeneously by the plastic strain of the UFG constituent, which is in contrast to the early strain localization and failure observed in the quasi-static loading condition.

The plastic interaction of the grains in the UFG region with the embedded B_4C particles is illustrated in Fig. 5 and Fig. 6, which compare the as-processed microstructure with that after dynamic deformation. The texturing and aspect ratio in the as-processed condition (Fig. 5) derive primarily from the extrusion process that the material experiences. In contrast, after dynamic deformation (Fig. 6), the grains in the UFG region are no longer well aligned and the aspect ratio has decreased by 10 pct. The grains in the UFG region appear to have deformed around the contour of the B_4C particles, as indicated by the white arrows in Fig. 6a and b.

The differences between the as-processed and dynamically deformed microstructures are highlighted in the schematics (Fig. 5 and Fig. 6). The elliptical shape of the grains in the schematics (Fig. 5 and Fig. 6) is representative of the aspect ratio in the UFG region. Quantitative comparison of these microstructures indicates that the average grain size in the UFG region increases by 53 nm after dynamic deformation relative to that of the as-processed material. This represents more than a 30 pct. increase in average grain size. A net grain coarsening is also clearly indicated in the grain size distribution histograms (Fig. 5 and Fig. 6). Grain coarsening after dynamic deformation has been previously observed in Al 6061 reinforced with Al_2O_3 particulate, and is attributed to the adiabatic heating that occurs during the high strain deformation test [31] and [32]. Therefore the grain coarsening as well as the texture development surrounding the B_4C reinforcement is indicative of plastic deformation in the UFG region. Note that grain coarsening in the UFG region also provides an explanation for the strain softening that is observed during dynamic deformation (Fig. 1).

Please cite this article as: R. Vogt, Z. Zhang, E. Huskins, B. Ahn, S. Nutt, K.T. Ramesh, E.J. Lavernia, J.M. Schoenung "**High strain rate deformation and resultant damage mechanisms in ultrafine-grained aluminum matrix composites**" Mater Sci & Engrg A 527 (2010) 5990-5996. DOI<http://dx.doi.org/10.1016/j.msea.2010.05.092>

5. Conclusions

The multi-component boron carbide-reinforced ultrafine-grained aluminum composite exhibited different deformation behavior under quasi-static and dynamic loading conditions. Microscale kinking was observed in the dynamically deformed samples, and polished sections prepared without abrasives revealed the development of axial microcracks in the matrix during dynamic loading. In the samples tested in the dynamic strain rate regime, the density of axial microcracks was significantly greater than that in samples tested in the quasi-static regime. Furthermore, the cracks in the dynamically tested samples did not coalesce. The absence of crack coalescence allowed the plastic strain in the UFG constituent to provide a significant increase in overall strain deformation. In addition, grain growth, attributed to adiabatic heating during dynamic loading, was observed and the composites showed strain softening in the dynamically tested samples. In the quasi-static strain rate regime, the mechanical behavior exhibited nearly perfect elastic deformation, and early strain localization led to the coalescence of microcracks and failure at small strains.

Acknowledgements: This research was sponsored by the U.S. Army Research Laboratory (ARL) and was completed under Cooperative Agreements W911NF-08-2-0028 and W911NF-06-2-0006. The views and conclusions made in this document are those of the authors and should not be interpreted as representing the official policies, either expressed or implied, of ARL or the U.S. Government. The U.S. Government is authorized to reproduce and distribute reprints for Government purposes notwithstanding any copyright notation hereon. The authors are grateful to JEOL USA, Inc. for providing access to the SM-09010 Cross Section Polisher.

Please cite this article as: R. Vogt, Z. Zhang, E. Huskins, B. Ahn, S. Nutt, K.T. Ramesh, E.J. Lavernia, J.M. Schoenung "**High strain rate deformation and resultant damage mechanisms in ultrafine-grained aluminum matrix composites**" Mater Sci & Engrg A 527 (2010) 5990-5996. DOI<http://dx.doi.org/10.1016/j.msea.2010.05.092>

References:

1. M.A. Meyers, A. Mishra, D.J. Benson, Prog. Mater. Sci., 51 (4) (2006), pp. 427–556
2. D.B. Witkin, E.J. Lavernia, Prog. Mater. Sci., 51 (1) (2006), pp. 1–60
3. C.C. Koch, D.G. Morris, K. Lu, A. Inoue, Mrs Bull., 24 (2) (1999), pp. 54–58
4. S.P. Joshi, K.T. Ramesh, B.Q. Han, E.J. Lavernia, Metall. Mater. Trans. A, 37A (8) (2006), pp. 2397–2404
5. R.G. Vogt, Z. Zhang, T.D. Topping, E.J. Lavernia, J.M. Schoenung, J. Mater. Process. Technol., 209 (11) (2009), pp. 5046–5053
6. H. Luo, L. Shaw, L.C. Zhang, D. Miracle, Mater. Sci. Eng. A, 409 (1–2) (2005), pp. 249–256
7. J. Ye, B.Q. Han, Z. Lee, B. Ahn, S.R. Nutt, J.M. Schoenung, Scr. Mater., 53 (5) (2005), pp. 481–486
8. J.C. Ye, J.H. He, J.M. Schoenung, Metall. Mater. Trans. A, 37A (10) (2006), pp. 3099–3109
9. Y. Wang, M. Chen, F. Zhou, E. Ma, Nature, 419 (6910) (2002), pp. 912–915
10. Y. Li, Y.H. Zhao, V. Ortalan, W. Liu, Z.H. Zhang, R.G. Vogt, N.D. Browning, E.J. Lavernia, J.M. Schoenung, Mater. Sci. Eng. A, 527 (1–2) (2009), pp. 305–316
11. H. Zhang, J. Ye, S.P. Joshi, J.M. Schoenung, E.S.C. Chin, K.T. Ramesh, Scr. Mater., 59 (10) (2008), pp. 1139–1142
12. H.T. Zhang, J.C. Ye, S.P. Joshi, J.M. Schoenung, E.S.C. Chin, G.A. Gazonas, K.T. Ramesh, Adv. Eng. Mater., 9 (5) (2007), pp. 355–359
13. J.Y. Lee, K.H. Han, J.M. Park, K. Chattopadhyay, W.T. Kim, D.H. Kim, Acta Mater., 54 (19) (2006), pp. 5271–5279
14. D.R. Chichili, K.T. Ramesh, Int. J. Solids Struct., 32 (17/18) (1995), pp. 2609–2626
15. T. Pardoen, Y. Brechet, Philos. Mag., 84 (3) (2004), pp. 269–297
16. M.F. Ashby, S.D. Hallam, Acta Metall., 34 (3) (1986), pp. 497–510
17. K.T. Ramesh, R.S. Coates, Metall. Trans. A, 23 (9) (1992), pp. 2625–2630
18. Y.F. Xue, H.N. Cai, L. Wang, F.C. Wang, H.F. Zhang, Z.Q. Hu, Compos. Sci. Technol., 68 (15–16) (2008), pp. 3396–3400
19. A.M. Lennon, K.T. Ramesh, Mater. Sci. Eng. A, 276 (1–2) (2000), pp. 9–21
20. S. Nemat-Nasser, H. Horii, J. Geophys. Res., 87 (1982), p. p6805
21. M.J. Hadianfard, R. Smerd, S. Winkler, M. Worswick, Mater. Sci. Eng. A, 492 (1–2) (2008), pp. 283–292
22. Y.F. Xue, H.N. Cai, L. Wang, F.C. Wang, H.F. Zhang, Mater. Sci. Eng. A, 445–446 (2007), pp. 275–280
23. B. Paliwal, K.T. Ramesh, J. Mech. Phys. Solids, 56 (3) (2008), pp. 896–923
24. C.M. Cady, G.T. Gray, Mater. Sci. Eng. A, 298 (1–2) (2001), pp. 56–62
25. M. Güden, O. Akil, A. Tasdemirci, M. Çiftçioglu, I.W. Hall, Mater. Sci. Eng. A, 425 (1–2) (2006), pp. 145–155
26. M. Guden, I.W. Hall, Comps. Struct., 76 (1–3) (2000), pp. 139–144
27. C.C. Poteet, I.W. Halla, Mater. Sci. Eng. A, 222 (1) (1997), pp. 35–44
28. M. Guden, I.W. Hall, J. Mater. Sci., 33 (13) (1998), pp. 3285–3291
29. B. Budiansky, N.A. Fleck, J.C. Amazigo, J. Mech. Phys. Solids, 46 (9) (1998), pp. 1637–1653
30. G. Ravichandran, G. Subhash, Int. J. Solids Struct., 32 (17–18) (1995), pp. 2627–2646
31. Q. Li, Y.B. Xu, Z.H. Lai, L.T. Shen, Y.L. Bai, Mater. Sci. Eng. A, 276 (1–2) (2000), pp. 250–256
32. G.M. Owolabi, A.G. Odeshi, M.N.K. Singh, M.N. Bassim, Mater. Sci. Eng. A, 457 (1–2) (2007), pp. 114–119

Please cite this article as: R. Vogt, Z. Zhang, E. Huskins, B. Ahn, S. Nutt, K.T. Ramesh, E.J. Lavernia, J.M. Schoenung "**High strain rate deformation and resultant damage mechanisms in ultrafine-grained aluminum matrix composites**" Mater Sci & Engrg A 527 (2010) 5990-5996. DOI<http://dx.doi.org/10.1016/j.msea.2010.05.092>

Please cite this article as: R. Vogt, Z. Zhang, E. Huskins, B. Ahn, S. Nutt, K.T. Ramesh, E.J. Lavernia, J.M. Schoenung "**High strain rate deformation and resultant damage mechanisms in ultrafine-grained aluminum matrix composites**" Mater Sci & Engrg A 527 (2010) 5990-5996. DOI<http://dx.doi.org/10.1016/j.msea.2010.05.092>